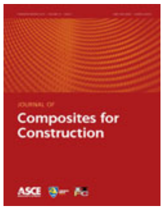

Journal of Composites for Construction

ISSN (print): 1090-0268
ISSN (online): 1943-5614
Publisher: American Society of Civil Engineers

Concrete Walls with Cutout Openings Strengthened by FRP Confinement

Cosmin Popescu, Gabriel Sas, Thomas Blanksvärd, and Björn Täljsten

Concrete walls with cutout openings strengthened by FRP confinement

Cosmin Popescu, S.M.ASCE[1]; Gabriel Sas[2]; Thomas Blanksvärd[3]; and Björn Täljsten[4]

[1] Ph.D. Candidate, Northern Research Institute – NORUT, Rombaksveien E6-47, N-8517 Narvik, Norway (corresponding author). E-mail: cosmin.popescu@norut.no

[2] Associate Senior Lecturer, Dept. of Civil, Environmental and Natural Resources Engineering, Luleå Univ. of Technology, 971 87, Luleå, Sweden

[3] Senior Lecturer, Dept. of Civil, Environmental and Natural Resources Engineering, Luleå Univ. of Technology, 971 87, Luleå, Sweden

[4] Professor, Dept. of Civil, Environmental and Natural Resources Engineering, Luleå Univ. of Technology, 971 87, Luleå, Sweden

Abstract

Redesigning buildings to improve their space efficiency and allow changes in use is often essential during their service lives to comply with shifts in living standards and functional demands. This may require the introduction of new openings in elements such as beams, walls and slabs, which inevitably reduces their structural performance, and hence necessitates repair or strengthening. However, there are uncertainties regarding both the effects of openings and the best remedial options. Here the authors report on an experimental investigation of the effectiveness of fiber-reinforced polymer (FRP)-based strengthening for restoring the axial capacity of a solid reinforced concrete wall after cutting openings. Nine half-scale specimens, designed to represent typical wall panels in residential buildings with and without door-type openings, were tested to failure. FRP-confinement and mechanical anchorages increased the axial capacity of walls with small and large openings (which had 25% and 50% reductions in cross-sectional area, respectively) by 34-50% and 13-27%, to 85-94.8% and 56.5-63.4% of their pre-cutting capacity, respectively.

Author keywords: Strengthening, Fiber-reinforced polymers, Concrete walls, Openings, Axial strength, Eccentricity, Mechanical anchorages, Confinement, Disturbed regions

Introduction

Openings in reinforced concrete (RC) structural elements such as beams, slabs or walls are often needed for technical or functionality reasons, i.e. to improve their space efficiency and/or meet shifts in functional requirements. However, openings have clear negative effects, as addressed in numerous studies – recent examples include (Mohammed et al. 2013, Floruţ et al. 2014, Todut et al. 2014, Popescu et al. 2016) – through the introduction of disturbed regions that significantly decrease the elements' ultimate load capacity, stiffness and energy dissipation. Thus, effects of any opening must be carefully considered in design stages, and addressed by specifying appropriate reinforcement detailing around the edges. However, when openings must be introduced in structures that have already been built the scope for such detailing is very limited. Instead, repair is often required (defined here as actions that fully or partially restore the structure's load-carrying capacity). New repair options are being developed and applied, but both further development of innovative approaches and more knowledge of their effects is needed.

European (EN1992-1-1 2004) and Australian (AS3600 2009) design codes provide some guidance regarding the design of walls with openings subjected to vertical loads. Both assume that the effects of a “small” opening (with area and height less than 1/10 and 1/3 of the wall’s total area and height, respectively) on the structural integrity of the element can be neglected if the wall is restrained on all sides. For a “large” opening exceeding these proportions, each remaining portion should be separately considered. The portion between a restraining member and opening should be treated as a separate member, supported on three sides, while areas between openings (if there are more than one) must be treated as being supported on two sides. Several other empirical models have also been proposed (Saheb and Desayi 1990, Doh and Fragomeni 2006, Guan 2010), calibrated using data from limited numbers of one-way (OW) and two-way (TW) action tests, with loading eccentricity up to one sixth of the wall thickness (Popescu et al. 2015). One-way and two-way action refer here to cases where, due to eccentricity, flexure occurs in one and two directions, respectively, as in panels restrained along the top and bottom edges (which develop out-of-plane curvature parallel to the load direction), and panels restrained along three or four sides (which generally deform in both horizontal and vertical directions).

The aim of the study presented here was to contribute to efforts to develop a convenient new repair system that can substantially restore the axial strength of concrete walls after openings have been cut. Traditionally RC walls with openings have been strengthened by either installing a frame around the openings using RC/steel members (Engel n.d.) or increasing the elements’ cross-sectional thickness (Delatte 2009). Nowadays, intervention in existing buildings must be minimal in order to minimize inconvenience due to limitations in use of the structure during repairs. An option is to use externally bonded fiber-reinforced polymers (FRP). This has been successfully tested by several authors in seismic retrofitting contexts (Demeter 2011, Li et al. 2013, Todut et al. 2015, Mosallam and Nasr 2016). Thus, the strengthening schemes proposed in the cited studies may not be suitable for repairing gravitationally loaded walls, and more research regarding their effects on elements' responses to vertically applied loads is required (Popescu et al. 2015).

The performance of non-seismically designed walls with openings strengthened with FRP has only been examined by Mohammed et al. (2013), who strengthened OW, 1/3-scale RC walls with openings varying in size from 5% to 30% of the total wall area by placing carbon FRP (CFRP) sheets around edges of the openings. As expected, the walls' load-carrying capacity increased as the principal stresses on the opening corners decreased. A limitation of the study by Mohammed et al. (2013) was that it only involved OW walls with no strengthening procedures for walls in TW action. Furthermore, the failure mode (concrete crushing) of unstrengthened TW walls with openings observed in experimental tests (Popescu et al. 2016) indicates that the strengthening configuration proposed by Mohammed et al. (2013) would not be suitable for them, and a better strengthening solution may be confinement.

Confinement with FRP has proved to be an efficient strategy for enhancing the strength and ductility of axially loaded members, although its effects are the most effective only for elements with circular cross-sections. For elements with rectangular cross-sections only parts of the cross-section are effectively confined (Mirmiran 1998, Pessiki 2001, Wu and Wei 2010, Liu et al. 2015). Design/analysis-oriented models developed by various researchers, reviewed by (Lam and Teng 2003, Rocca et al. 2008), have shown that as the aspect ratio of the cross-section increases the enhancement of compressive strength provided by FRP-confinement decreases. Members with aspect ratios higher than 3:1 are usually regarded as wall-like columns. Creating a new opening in a concrete wall inevitably increases the aspect ratio of the remaining portions, hereafter piers (or wall-like column), and reduces the effectiveness of FRP-confinement. Few studies have addressed this problem. However, it has been shown that the axial strength and ductility of short (1.5 m) columns with an aspect ratio of 3.65 to 1 can be increased by confinement using longitudinal and transversal FRP sheets in combination with placing fiber anchor spikes along the wider faces of the column (Tan 2002) or adding semi-cylindrical attachments (high-strength mortar) to increase the cross-sectional area (Tanwongsval et al. 2003). In addition, quadri-directional CFRP can improve seismic performance, but not other strength parameters, according to (Prota et al. 2006). Adding heavy anchor spikes or cross-sectional enlargement with high-strength mortar can also double the confining effect of circumferential FRP, but excessively light fiber anchor spikes fail prematurely and thus have little effect on strength, relative to controls with no anchors (Triantafillou et al. 2015). In contrast to these findings, De Luca et al. (2013) found that confining wall-like columns with an aspect ratio of 2.92 to 1 with FRP (but no longitudinal or anchor fibers) could enhance the axial ductility, but not axial capacity. Hence it is necessary to use a hybrid method (FRP-confinement and longitudinal FRP fibers, anchors or increases in cross-section) when it is necessary to increase both the axial strength and ductility of wall-like columns.

Before such an approach can be used with confidence more information about response of the overall system is required. Hence, in the presented study the effectiveness of FRP-confinement with mechanical anchorages for increasing the axial strength of concrete walls weakened by cut-out openings was investigated. Increases in axial strength, ductility, steel reinforcement and FRP strain utilization were measured to improve understanding of such elements' structural behavior. The results provide information that it is believed will assist efforts to develop a new design model capable of capturing complicating effects such as load eccentricity and large aspect ratios of elements' cross-sections.

Experimental testing

Specimen design and test matrix

Half-scale walls designed to represent typical wall panels in residential buildings with and without cut-out openings (1800 mm long, 1350 mm wide and 60 mm thick), were constructed for testing to failure. The specimens are designed to carry vertical loads with no transverse loads between supports or lateral in-plane forces. The walls were tested in TW action and subjected to axial loading with small eccentricity (1/6 of the wall thickness), as typically found in practice and applied in previous studies. Moreover, the simplified design formulas found in the literature were calibrated for eccentricity up to one sixth of a wall's thickness to ensure that the resultant axial force passes through the middle-third of the wall's overall thickness. Thus, the selected eccentricity facilitates comparison of results with those of previous tests and further development of published equations.

Minimum wall reinforcement was provided according to American and Australian design codes (ACI 318 2011, AS3600 2009). In the European code (EN1992-1-1 2004) such specimens are treated as lightly reinforced or un-reinforced elements, as the sections contain reinforcement placed within a single layer, thus not contributing to the overall capacity. Consequently, welded wire fabric reinforcement was used to reinforce the walls, consisting of deformed 5 mm diameter bars with 100 mm spacing in both orthogonal directions and centrally placed in a single layer. The vertical and horizontal steel reinforcement ratios resulting from this configuration are 0.327 and 0.339%, respectively. The specimens with openings were detailed to replicate solid walls with sawn cut-outs, i.e. no additional reinforcement was placed around the edges or corners of the openings. More details about the fabrication process are given in Popescu et al. (2016).

The test matrix can be divided into three stages, designated I-III, in which reference (unstrengthened) specimens, pre-cracked specimens strengthened by FRP and uncracked specimens strengthened by FRP (duplicated to increase the reliability of the data) were tested, respectively.

Three specimens were loaded to failure in stage I: a solid panel, a panel with a “small” symmetric half-scaled single door-type opening (450 × 1050 mm), and a panel with a “large” symmetric half-scaled double door-type opening (900 × 1050 mm). The specimens’ dimensions and reinforcement details are presented in Fig. 1. The small and large openings represent 25 and 50% reductions, respectively, in the cross-sectional area of the solid wall. Thus, these tests enabled evaluation of effects of introducing new openings in a solid wall. The damage level was evaluated in terms of ultimate load, crack pattern, displacement profiles, strains in concrete and steel reinforcement, ductility, and energy release at failure.

In stage II, two specimens (one with a small opening and one with a large opening) were first loaded to the point required to create a significant crack based on nonlinear finite element analyses and observations of the reference specimens in stage I. Of course, the significance of a crack depends on many factors, including the building’s functions and environmental exposure. However, according to ACI 224R-01 (2001) a crack wider than 0.15 mm may require repair. To create cracks of this width the specimens were loaded up to 75% of their unstrengthened axial capacity. They were subsequently completely unloaded then strengthened by FRP and tested to failure. This procedure mimics scenarios in which the creation of openings and subsequent presence of a sustained load results in degradation of a wall. In stage III duplicated specimens with openings of each size were strengthened with the FRP system in an uncracked state then loaded to failure.

For convenience, the specimens are designated according to the stage when they were tested (I, II or III), their type (C, S or L: for solid wall, and walls with small and large openings, respectively) and (for specimens used in stage III) serial number. It should be noted that “small” and “large” are used here as convenient designations rather than as clearly delimited terms with specific thresholds and implications.

CFRP strengthening

Design method

Information obtained from analysis of failure modes of unstrengthened walls reported by Popescu et al. (2016) was used to identify a suitable FRP configuration. In all cases, the walls had a brittle failure due to crushing of concrete with spalling and reinforcement buckling (see Fig. 2). In order to increase the axial strength of walls with openings, confinement strengthening was designed as follows. First, the decrease in capacity caused by introducing new openings was found by testing the unstrengthened elements. The results indicate that the 25% and 50% reductions in cross-sectional area of the solid wall caused by introducing the small and large opening reduced the load carrying capacity by nearly 36% and 50%, respectively. In order to regain the loss of capacity, two choices were available: increasing the specimen’s thickness or the concrete compressive strength through confinement. Increasing the concrete compressive strength through FRP-confinement was the focal aspect of the work presented here.Next, the EC2 (EN1992-1-1 2004) design model for TW walls (Eq. (1)) was used to find the confined compressive strength (f_{cc}) needed to restore the capacity of the solid wall.

$$N_{I-C} = 2 f_{cc} L_{pier} t \Phi \tag{1}$$

where

$$\Phi = 1.14\left(1 - 2\frac{e+e_a}{t}\right) - 0.02 \cdot \frac{H_{eff}}{t} \le \left(1 - 2\frac{e+e_a}{t}\right) \tag{2}$$

Here: N_{I-C} is the experimentally obtained axial capacity of a solid wall, t is the wall thickness, L_{pier} is the length of a pier; f_{cc} is the theoretical compressive strength of the confined concrete; e is the initial eccentricity, $e = t/6$; and e_a is an additional eccentricity due to lateral deflection of the wall. The additional eccentricity, e_a, accounts for the effect of slenderness, also known as second order (or P–Δ) effects, and can be computed using the EC2 approach; $e_a = H_{eff}/400$.

with $H_{eff} = \beta H$ being the effective height. Values for the effective height factor β are given for the most commonly encountered restraints:

$$\beta = \begin{cases} \dfrac{1}{1+\left(\dfrac{H}{3L}\right)^2} & \text{three-sides} \\ \dfrac{1}{1+\left(\dfrac{H}{L}\right)^2} & \text{four-sides with } L \ge H \\ \dfrac{L}{2H} & \text{four-sides with } L < H \end{cases} \tag{3}$$

Solving Eq. (1) yields a ratio between the confined and unconfined compressive strength, f_{cc}/f_c, of about 1.26 and 1.44 for walls with small and large openings, respectively. The resulting value was then used in conjunction with the model presented by Lam and Teng (2003) to estimate the required thickness of FRP jacket.

For FRP-wrapped rectangular concrete columns, Lam and Teng (2003) proposed an analytical relationship, Eq. (4), which considers the effect of non-uniformity of confinement through a shape factor (k_{s1}):

$$\frac{f_{cc}}{f_c} = 1 + k_1 k_{s1} \frac{f_l}{f_c} \tag{4}$$

where f_c is compressive strength of the unconfined concrete, f_{cc} is compressive strength of the confined concrete; k_1 = 3.3 is the confinement effectiveness coefficient and f_l is confining pressure.

The shape factor, k_{s1}, is defined as:

$$k_{s1} = \left(\frac{b}{h}\right)^2 \frac{A_e}{A_c} \tag{5}$$

The effective confinement area ratio A_e/A_c is calculated as:

$$\frac{A_e}{A_c} = \frac{1 - \left[\left(b/h\right)(h-2R)^2 + (h/b)(b-2R)^2\right]/3A_g - \rho_{sc}}{1-\rho_{sc}} \tag{6}$$

where b and h are width and height of the cross-section, respectively, A_e is effective confinement area, A_c is total area of the cross-section, R is corner radius, ρ_{sc} is cross-sectional area proportion of longitudinal steel, and A_g is gross area of the column section with rounded corners.

The confining pressure, f_l, is given by:

$$f_l = \frac{2 \cdot f_{frp} \cdot t_{frp}}{D'} = \frac{2 \cdot f_{frp} \cdot t_{frp}}{\sqrt{h^2 + b^2}} \tag{7}$$

where f_{frp} and t_{frp} are the tensile strength and thickness of the FRP jacket, respectively.

As the model is not valid for members with high cross-section aspect ratios the following procedure was employed. The transverse fiber sheets were fixed using steel bolts in a configuration that created virtual cross-sections with an aspect ratio limited to 2:1 (60 x 120 mm starting from the edge of the opening, see Fig. 3). Following the assumption by Tan (2002), that such internal transverse links provide additional anchor points for FRP jackets, the effectively confined area for pure compression is shown in Fig. 3. One virtual column strip was extracted so that Eq. (6) would be applicable; the results were then extrapolated to the rest of the wall-pier. Based on required thicknesses of FRP layers under these conditions back-calculated from Eq. (7), two and three 0.17 mm thick FRP layers were used to strengthen the specimens with small and large openings, respectively. The authors are aware that loading eccentricity (included in the tests to mimic imperfections in routine construction practices), may reduce the effectiveness of the confinement, but the lack of better models prevented the incorporation of appropriate parameters to simulate its effects. Thus, as noted by Mukherjee (2004) more tests are required to extend current confinement models to account for loading imperfections.

Analyzing the failure mechanism of the unstrengthened specimens the authors could not see any decisive failure of the beam above the opening except some small cracks. The same amount of FRP layers as for wall-piers were conservatively used to strengthen the beam above the opening in order to redirect the load towards wall-piers. The FRP material was placed along both lateral faces from edge to edge of the wall and bent under the bottom part of the beam.

Specimen preparation and material properties

The walls were cast in a long-line form, in lying position resting on a steel platform that can accommodate up to five specimens, in two batches: the specimens used in stages I and II in the first batch, and those used in stage III in the second batch. The concrete used to cast the specimens was a self-consolidating mix that could be poured without vibrating it, including dynamon NRG-700, a superplasticizer added to provide high workability and early strength. To determine mechanical characteristics of the concrete (compressive strength and fracture energy), five cubes and beams from each batch with standardized sizes were cast and cured in identical conditions to the specimens. The average cubic compressive strength of the concrete was determined in accordance with (SS-EN 12390-3:2009 2009) while the fracture energy was determined following recommendations in RILEM TC 50-FMC (1985). In addition, five coupons were taken from the reinforcing steel meshes and tested according to SS-EN ISO 6892-1:2009 (2009) to determine their stress-strain properties. The results (means and corresponding coefficients of variation, CoV) are given in Table 1.

Temporary timber supports were created for all six specimens to replicate the vertical positions of the elements in a structure and provide access around the specimens. The concrete surfaces were prepared by grinding and cleaning with compressed air (see Fig. 3a-b). The corners adjacent to the opening edge were rounded with a corner radius of 25 mm to avoid premature failure of the FRP and increase the effect of confinement. The strength enhancement relies on the continuity (fully wrapped) of the fiber sheets in the transverse direction. The as-built boundary conditions limited access to lateral edges of the cross-section. Therefore, the authors applied U-shaped CFRP sheets fixed with mechanical anchorages, installed in 8 mm holes drilled through the wall at positions pre-marked on the concrete surface.

The sheets were applied using the wet lay-up procedure as illustrated in Fig. 4c-d. A two-component epoxy primer (StoPox 452 EP) was applied to the prepared surfaces of the specimens, while CFRP (StoFRP IMS300 C300) sheets were impregnated with StoPox LH two-component epoxy resin (elastic modulus, 2 GPa) then applied approximately 6 hours later. These sheets have uni-directional fibers with an areal weight of about 300 g/m^2, high tensile strength (5500 MPa) and intermediate elastic modulus (290 GPa) according to the supplier. The ultimate tensile elongation of the fibers was about 19‰.

The specimens were stored indoors at around 18°C for about 7 days to allow the epoxy resin to cure. The surface of each specimen surface was then locally heated with a heat gun and a thermal imaging camera (FLIR T620bx, FLIR Systems, Wilsonville, Oregon) was used to look for areas with poor adhesion or air voids (none were detected) and find the pre-drilled holes (Fig. 4e). Steel anchorage bolts, M6S 8.8 – SS-EN ISO 4014 (2011), were then inserted into pre-drilled holes and prestressed with a torque estimated from the clamp load as 75% of the proof load as specified in SS-EN ISO 898-1 (2013). It was believed that by prestressing the steel bolts would increase the strengthening performance by providing an active confinement as suggested by Harajli and Hantouche (2015). Neoprene padding was placed between the 50 mm steel washers providing the anchorage and CFRP to avoid shearing of the fibers. The whole strengthening process is illustrated in Fig. 4. The strengthening entirely covers the concrete surface, so humidity and moisture issues may arise. However, the panels used in this study were intended to mimic indoor elements, classified as environmental Class 0 (i.e. structures located in a dry environment with low humidity) according to Täljsten (1999). The strengthening was applied without any sustained load due to permanent and partly due to imposed load.

Test setup and instrumentation

All specimens were tested gravitationally in a test-rig designed to represent the as-built boundary conditions (Fig. 5). The test rig had to simulate hinged connections at the top and bottom edges of the specimen. The side edges were restrained to simulate TW effects for real transverse walls under as-built conditions that permitted rotation but prevented translation

(Section 1-1 in Fig. 5). The axial load was applied eccentrically (at 1/6 of the wall thickness) in increments of 30 kN/min with inspection stops every 250 kN to monitor cracks in the specimens. The eccentricity was induced by a 22 mm diameter steel rod welded to each loading beam (HEB220). Four hydraulic jacks, each with a maximum capacity of 1.4 MN (1 MN (MegaNewton) = 10^6 N), were networked together to apply a uniformly distributed load along the wall length. A general view of the test setup is shown in Fig. 6.

Out-of-plane and in-plane displacements were monitored using linear displacement sensors, and strain gauges intercepting potential yield lines (obtained from nonlinear finite element analysis) were installed on the steel reinforcement and CFRP. Data obtained from the strain gauges and linear displacement sensors were then supplemented by measuring full-field strain distributions, using digital image correlation (DIC) technique. Several studies have shown that DIC methodology can provide stable and reliable strain and displacement measurements in both laboratory environments (Smith 2011, Mahal et al. 2015) and field tests (Sas et al. 2012). A system (GOM mbH) capable of capturing three-dimensional displacements was then used to facilitate the DIC measurements. The area of each specimen monitored by the optical DIC system was the right-upper corner on the tension side (780 mm x 660 mm, see Fig. 7), an area of particular interest for monitoring strain and crack development in discontinuous regions. Patterning of the monitored surfaces (required for this equipment) was applied using a stencil and spray for unstrengthened specimens, and manually for strengthened elements since access to the surface was obstructed by the anchorages. A regular pattern was obtained when the stencil was used, while a random pattern was manually applied. To avoid interference with the optical measurement system the reinforcement and outer FRP layer were only instrumented with strain gauges on half of each specimen (the left pier, on the tension side), as permitted by the symmetry of the test set-up. The instrumentation scheme for walls with openings is shown in Fig. 7. The arrangement of the monitoring system for the solid wall differed, but the position of D1 was identical to enable comparison of all specimens.

Test results and discussion

Tests on reference specimens. Stage I

This section briefly summarizes results from stage I, i.e. tests with reference specimens, which behaved typically for elements restrained on all sides, deflecting in both horizontal and vertical directions. The displacements were generally symmetric, but there were some asymmetries due to variations in material properties. All specimens failed by concrete crushing with spalling and reinforcement buckling. Cracks opened late in the loading of the solid wall (at 85% of the peak load), and earlier in the loading of specimens with both small and large openings (at 50% and 20% of peak load, respectively). The peak loads are presented in Table 2, and the effects of opening size in the load-displacement curves for the three specimens (recorded at the same position, D1 and symmetric to D1 on the other pier) shown in Fig. 8. Crack pattern at failure is shown in Fig. 2 for both tension and compression side of the specimens. Strain responses in steel reinforcement and concrete were also recorded and are given elsewhere (Popescu et al. 2016), but strains in the reinforcement at selected load levels are given in comparison with those from strengthened specimens to evaluate the strain utilization.

Tests on strengthened specimens. Stages II & III

Pre-cracking

The specimens used in stage II were loaded up to 75% of the reference walls' axial capacity. At this point the strains recorded in the steel reinforcement were lower than yielding. The maximum values were -0.63‰ (compressed bar) and 0.43‰ (tensioned bar) for the specimen with a small opening and -0.91‰ and 2.25‰ for the specimen with a large opening. A few cracks were observed, mainly in the spandrel above the opening followed by other diagonal cracks from the bottom corner of the wall with approximately 50° inclination, similar to those reported for the reference specimens. When the target damage (pre-cracking) level was reached, the specimens were completely unloaded and removed from the test setup to apply the strengthening. Thus the pre-cracks were nearly closed during this manipulation.

Failure modes

No cracks could be seen in the following loading cycles because the specimens were fully covered by FRP sheets. Thus, in contrast to the reference specimens, for which increases in deformations and cracking provided clear visual warnings of imminent failure, sounds provided more warnings of the imminent failure of strengthened specimens. Crushing of the concrete accompanied by debonding of the FRP sheets occurred at failure. In all but one of the tests (III-S2, see below) the primary failure occurred at the bottom of one of the piers, and was immediately followed by bulging of the FRP on the diagonally opposite side, i.e. the region around the opening's corner. The debonding of the FRP started in regions between steel anchorage rows (see Fig. 9), highlighting the need for vertical strips or even bi-directional fibers to improve utilization of the CFRP fibers and further increase the element's axial strength.

After each test the FRP sheets were removed to observe crack patterns. None were detected part from those located around the failure region. However, as already mentioned, specimen III-S2 had a different failure mode, with crushing of concrete and debonding of the FRP along the line between the wall corner and opening corner of one pier (Fig. 9c). After stripping the FRP jacket (Fig. 9c) another diagonal crack was revealed on the spandrel starting from the re-entrant corner. The failure modes of all specimens, both pre-cracked and un-cracked, were similar.

Axial load versus displacements response

Fig. 10 shows load-displacement data recorded at the D1 location (identical for all specimens) of both strengthened and reference elements. As shown in Table 2, the strengthening increased maximum loads at failure of pre-cracked specimens with small and large openings by 49% and 27%, respectively. Slightly lower increases were observed for uncracked specimens: 45% and 34% for specimens III-S1 and III-S2 with small openings, respectively, and 13% and 26% for specimens III-L1 and III-L2 with large openings, respectively. Thus, FRP strengthening seems to be most effective for pre-cracked elements. The FRP strengthening also changed the initial stiffness of the elements, but less for the pre-cracked specimens than for uncracked specimens. Similar behavior was reported by Wu et al. (2014) for FRP-confined concrete cylinders with varying damage levels.

The increase in axial strength and initial stiffness of specimen III-L1 were relatively low due to an error during the test. The lateral bracing of the test rig was designed to be connected to the foundation support through slotted holes, to account for variations in the thickness of the wall panels, thus allowing a little sliding of the entire system. The bolts were then prestressed to obtain high friction between the foundation support and lateral bracing elements. However, the bolts were accidentally loosened for specimen III-L1, thus friction was lost, permitting higher deformation of the specimen’s lateral edges. This was detected by analyzing the measurements on the lateral bracing system, which for the sake of brevity are not plotted here.

The strengthening did not increase the load carrying capacity of any of the specimens with openings to that of a solid wall. The axial strength of specimens with a small opening were between 85-94.8% of that of a solid wall (target I-C, Fig. 10), while the axial strength of specimens with a large opening were 56.5-63.4% of that of a solid wall (target I-C) and 88.9-99.8% of that of a wall with a small opening (target I-S, Fig. 10). The higher increase in capacity of specimens with a small opening can be attributed to the larger aspect ratios of the piers. Thus, both dilatation of concrete in compression and yield lines of the concrete in tension contribute to the increase in capacity.

Steel reinforcement and FRP strain responses

It was believed that the strengthening method would affect local performance measures such as demands on the steel reinforcement. Thus, before casting electrical resistance strain gauges with pre-attached lead wires were bonded to the reinforcement to monitor such demands. Selected strain values at certain loadings (50%, 75% and 100% of the peak load) are compared with those obtained for the reference specimens in Fig. 11 and Fig. 12. Unfortunately, the connections between some of these wires and the strain gauges were damaged during the strengthening process (e.g. grinding of the concrete surface). These gauges are indicated with asterisks in the figures.

The comparison is plotted as bar charts in Fig. 11 for pre-cracked, strengthened specimens and Fig. 12 for un-cracked, strengthened specimens. Overall, the FRP strengthening reduced strain in the steel reinforcement during the tests. It should be noted that Figs. 11 and 12 compare strains recorded at the same proportions of the specimens’ peak loads. Thus, as peak loads were higher for the strengthened specimens, the effectiveness of the strengthening in this respect was even greater than the figures visually indicate. Some of the strains recorded for reference specimens reached the yielding point at failure with buckling of the reinforcement, specifically of horizontal bars G4 and G6 located in the pier of the wall with a small opening, and G3 located in the midspan – bottom bar of the spandrel for the wall with large opening. Above the 75% load level the strains increased rapidly for all horizontal bars regardless of the opening size while a more gradual increase was observed for vertical bars. For strengthened elements the demands on the steel reinforcement were somewhat lower during the specimen loading, and more evident as failure approached. The strains in these cases gradually increased, with no sudden jumps or either yielding or buckling of the reinforcement. The amelioration provided by the FRP fibers is less evident for vertical bars because the fibers had been aligned only horizontally, and thus provided relatively little vertical contribution. Strains were reduced (relative to those in corresponding unstrengthened specimens) particularly strongly in the horizontal bar above the opening, and most strongly in the specimens with large openings since the stresses on the reinforcement (and hence utilization of the composite material) increase with increases in the spandrel's span. No noticeable differences in these observations were detected between pre-cracked and uncracked specimens.

Strains in the FRP of strengthened specimens at peak load were also recorded, as listed in Table 2, where (for instance) F1-T and F1-C indicate strains recorded at position "F1" in the wall's plane at tension and compression sides of the element, respectively (see Fig. 7). The tension side is defined as the specimens' surface where tensile cracks occur due to load eccentricity. In a hypothetical eccentrically loaded one-dimensional element strain gauges located on the compression side would register different strains compared to those located on the tension side. In the design process this effect of non-uniformity in strain efficiency was not taken into consideration, which may explain why lower than predicted ultimate loads were registered for the strengthened elements. On average, strains on the tension side were more than two times higher than the readings on the compression side for specimens with large openings and more than six times higher for specimens with small openings. The strain gauge located at the midspan of the spandrel (F5) recorded the highest strains, peaking at about 1.89‰.

It should be noted that these values are measured strains and not necessarily the highest in the specimens since the strain paths may have differed from those expected. Moreover, single point information is not as valuable as full-field information. Therefore, the authors also examined full-field surface displacements and transformed them into surface strain fields. To reduce the computation time, areas around the anchorages (slightly larger than in reality to avoid their contours complicating analysis) were masked and ignored. Major strains in other areas of each specimen at the peak load were plotted (Fig. 13a-h) to gain insights into the full strain field around the corner openings. Cracks were denser and more distinct in unstrengthened specimens (Fig. 13a and e), than in strengthened specimens, where they were more scattered. Furthermore, in all strengthened specimens the major strains tended to form a diagonal path through the spandrel, indicating that the arching effect cancelled by introducing the opening is re-activated through addition of strengthening material. This effect is clearest for walls with large openings. For unstrengthened specimens 3D-DIC also offers more detailed, and valuable, information on crack patterns than the one captured at failure shown in Fig. 2. This is partly because some cracks closed after failure and partly because hairline cracks are difficult to observe with the naked eye, especially during specimen loading.

Ductility factors and energy dissipation at failure

Displacement-based ductility factors (defined as the ratios between elastic and ultimate displacements recorded at D1, $\mu_{\Delta}=\delta_e/\delta_u$) were computed and are reported in Table 2. A simplified procedure proposed by Park (1988) was adopted to identify a distinct elastic displacement. The method assumes that the elastic displacement should be computed for an equivalent elasto-plastic system with reduced stiffness (arguably the most realistic approach for RC structures). The reduced stiffness is found as the secant stiffness related to 75% of the peak load and the horizontal plateau corresponding to the peak load of the real system (Fig. 8). The maximum displacement corresponds to the post-peak deformation when the load has decreased by 20% or the reinforcement buckles, whichever occurs first. In addition to ductility factors, energy dissipation (E_d) was also evaluated as the area under the load-displacement curves.

Neither ductility factors nor energy dissipation were improved by the strengthening with FRP. In fact, in most cases reductions were noted for the strengthened specimens in relation to the corresponding unstrengthened specimens. The introduction of the small and large openings in a solid wall resulted in similar, sharp reductions in computed ductility factors and energy dissipation. Perhaps, an alternative to avoid this drawback is to use textile-reinforced mortars (TRM). Tetta et al. (2016) reported that TRM jackets were more effective than FRP jackets considering the specimen's deformation capacity.

Conclusion and future work

The main conclusions drawn from the reported tests on the effectiveness of FRP-confinement of walls with cut-out openings can be briefly summarized as follows:

- Creating new openings in solid walls dramatically reduces their axial strength. The “small” and “large” openings in these tests resulted in 36% and 50% reductions, respectively. More tests are required, including walls with intermediate size openings, to identify optimal size thresholds and transition points between RC walls and RC frames in design codes for structural elements.
- The strengthening method increased the axial strength of specimens with small and large openings by 34-50% and 13-27% relative to that of corresponding unstrengthened specimens. However, the FRP strengthening method did not fully restore the axial strength of a solid wall in any of the tests. The type of FRP sheet used to strengthen the specimens was uni-directional, but bi-directional fibers or vertical strips may have been more effective. Also, anchoring the FRP sheets to the wall foundation and adjacent elements (i.e. transverse walls or floors) may delay debonding, thereby increasing the axial strength. The optimal distances between steel anchorages, and potential effects of the prestressing force of the bolts, should be further investigated.
- The strengthening did not avoid brittle failure, i.e. concrete crushing. However, it could avoid buckling of the reinforcement and the explosive failure mode observed in unstrengthened specimens.
- Reductions in energy dissipation and ductility factors of strengthened specimens, relative to corresponding unstrengthened specimens, reduce the system’s effectiveness.

The lateral restraints transformed the problem into a three-dimensional rather than one-dimensional problem. It is therefore necessary to develop a design model that can better describe current stress states. In this study the design of the FRP strengthening was based on one-dimensional element with no load eccentricity assumptions. However, it may be possible to develop disk theory (Nielsen 1999) to derive a theoretical model that provides better estimates of capacities of FRP-strengthened walls with openings.

Acknowledgements

The authors would like to acknowledge the Research Council of Norway (RFF), Development Fund of the Swedish Construction Industry (SBUF) and Skanska for financing the work in this project. Special thanks are due to the technicians of CompLab, the structural engineering laboratory at Luleå University of Technology (LTU). The authors would also like to express gratitude to others who provided help during this research program, including: Dr. Dan Diaconu from Politehnica University Timisoara for helping with the strengthening work, and PhD students Cristian Sabau and Niklas Bagge (both from LTU) for providing help with optical measurements and fruitful discussions, respectively.

Notations

The following symbols are used in this paper:

A_c = Cross-sectional area of concrete

A_e = effective confinement area

A_g = the gross area of a column section with rounded corners

E_d = energy dissipation

G_F = fracture energy

H= height of the wall

H_{eff} = effective height of the wall

L = length of the wall

L_{pier} = length of the wall-pier

N_{test} = peak load

$N_{I\text{-}C}$ = failure load of the solid wall

R = corner radius

b = width of a cross-section

e = test eccentricity

e_a = additional eccentricity

f_c = compressive strength of unconfined concrete

f_{cc} = compressive strength of confined concrete

f_{frp} = tensile strength of a FRP jacket

f_l = confining pressure

f_u = mean value of tensile strength of reinforcement

f_y = mean value of yield strength of reinforcement

h = height of the cross-section

k_1 = confinement effectiveness coefficient

k_{s1} = shape factor for strength enhancement

t_{frp} = thickness of a FRP jacket

β = effective height factor which depends on the support conditions

δ_e = elastic displacement

δ_u = ultimate displacement

ε_u = mean value of tensile strain of reinforcement

$\varepsilon_{u,frp}$ = strain in a FRP jacket

ε_y = mean value of yield strain of reinforcement

Φ = factor taking into account eccentricity, including second order effects and normal effects of creep

μ_Δ = ductility index

ρ_{sc} = cross-sectional area ratio of longitudinal steel

References

ACI 224R-01 (2001). "Control of Cracking in Concrete Structures." American Concrete Institute (ACI). ACI Committee 224.

ACI 318 (2011). "Building code requirements for structural concrete and commentary ", American Concrete Institute (ACI), Farmington Hills, MI.

AS3600 (2009). "Concrete structures." Standards Australia, Sydney, Australia.

De Luca, A., Nardone, F., Lignola, G., Prota, A., and Nanni, A. (2013). "Wall-Like Reinforced Concrete Columns Externally Confined by Means of Glass FRP Laminates." *Advances in Structural Engineering*, 16(4), 593-604.

Delatte, N. (2009). *Failure, Distress and Repair of Concrete Structures*, Woodhead Publishing Limited, Abington Hall, Granta Park, Great Abington, Cambridge CB21 6AH, UK.

Demeter, I. (2011). "Seismic retrofit of precast RC walls by externally bonded CFRP composites." PhD Thesis, Politehnica University of Timisoara, Timisoara, Romania.

Doh, J. H., and Fragomeni, S. (2006). "Ultimate load formula for reinforced concrete wall panels with openings." *Advances in Structural Engineering*, 9(1), 103-115.

EN1992-1-1 (2004). "Design of concrete structures – Part 1–1: General rules and rules for buildings." CEN (European Committee for Standardization), Brussels, Belgium.

Engel, P. (n.d.). "General rehabilitation techniques using steel." <http://www.constructalia.com/english/renovation_with_steel/ii_general_rehabilitation_techniques_using_steel#.VMPsNP6G9Wg>. (2016.05.05).

Floruţ, S.-C., Sas, G., Popescu, C., and Stoian, V. (2014). "Tests on reinforced concrete slabs with cut-out openings strengthened with fibre-reinforced polymers." *Composites Part B: Engineering*, 66C, 484–493.

GOM mbH "ARAMIS - Optical 3D Deformation Analysis." <http://www.gom.com/metrology-systems/system-overview/aramis.html>. (2016-05-05).

Guan, H., Cooper, C., and Lee, D.-J. (2010). "Ultimate strength analysis of normal and high strength concrete wall panels with varying opening configurations." *Engineering Structures*, 32(5), 1341-1355.

Harajli, M. H., and Hantouche, E. G. (2015). "Effect of Active versus Passive Confinement on Seismic Response of Wide RC Columns with Lap Splices." *Journal of Structural Engineering*, 141(9), 04014221.

Lam, L., and Teng, J. G. (2003). "Design-Oriented Stress-Strain Model for FRP-Confined Concrete in Rectangular Columns." *Journal of Reinforced Plastics and Composites*, 22(13), 1149-1186.

Li, B., Kai Qian, and Tran, C. T. N. (2013). "Retrofitting earthquake-damaged RC structural walls with openings by externally bonded FRP strips and sheets." *Journal of composites for construction*, 17(2), 259-270.

Liu, H.-X., Liu, G.-J., Wang, X.-Z., and Kong, X.-Q. (2015). "Effect of cross-sectional aspect ratio and basalt fiber-reinforced polymer-confined number on axial compression behavior of short columns." *Journal of Reinforced Plastics and Composites*, 34(10), 782-794.

Mahal, M., Blanksvärd, T., Täljsten, B., and Sas, G. (2015). "Using digital image correlation to evaluate fatigue behavior of strengthened reinforced concrete beams." *Engineering Structures*, 105, 277-288.

Mirmiran, A., Shahawy, M., Samaan, M., Echary, H., Mastrapa, J., Pico, O. (1998). "Effect of Column Parameters on FRP-Confined Concrete." *Journal of Composites for Construction*, 2(4), 175-185.

Mohammed, B., Ean, L. W., and Malek, M. A. (2013). "One way RC wall panels with openings strengthened with CFRP." *Construction & Building Materials*, 40, 575-583.

Mosallam, A. S., and Nasr, A. (2016). "Structural performance of RC shear walls with post-construction openings strengthened with FRP composite laminates." *Composites Part B: Engineering* (In Press).

Mukherjee, A., Boothby, T., Bakis, C., Joshi, M., and Maitra, S. (2004). "Mechanical Behavior of Fiber-Reinforced Polymer-Wrapped Concrete Columns—Complicating Effects." *Journal of Composites for Construction*, 8(2), 97-103.

Nielsen, M. P. (1999). *Limit analysis and concrete plasticity, Second Edition*, CRC Press, Boca Raton, FL.

Park, R. (1988). "State of the art report: ductility evaluation from laboratory and analytical testing." *Proceedings of Ninth World Conference on Earthquake Engineering., Vol. VIII,* Tokyo-Kyoto, Japan, 605-616.

Pessiki, S., Harries, K., Kestner, J., Sause, R., Ricles, J. (2001). "Axial Behavior of Reinforced Concrete Columns Confined with FRP Jackets." *Journal of Composites for Construction*, 5(4), 237-245.

Popescu, C., Sas, G., Blanksvärd, T., and Täljsten, B. (2015). "Concrete walls weakened by openings as compression members: A review." *Engineering Structures*, 89, 172-190.

Popescu, C., Sas, G., Sabău, C., and Blanksvärd, T. (2016). "Effect of cut-out openings on the axial strength of concrete walls " *Journal of Structural Engineering* (*In press), http://dx.doi.org/10.1061/(ASCE)ST.1943-541X.0001558*

Prota, A., Manfredi, G., and Cosenza, E. (2006). "Ultimate behavior of axially loaded RC wall-like columns confined with GFRP." *Composites Part B: Engineering*, 37(7–8), 670-678.

RILEM TC 50-FMC (1985). "Determination of the fracture energy of mortar and concrete by means of three-point bend tests on notched beams." *Materials and Structures*, 18(4), 287-290.

Rocca, S., Galati, N., and Nanni, A. (2008). "Review of design guidelines for FRP confinement of reinforced concrete columns of noncircular cross sections." *Journal of Composites for Construction*, 12(1), 80-92.

Saheb, M., and Desayi, P. (1990). "Ultimate strength of RC wall panels with openings." *Journal of Structural Engineering*, 116(6), 1565-1578.

Sas, G., Blanksvärd, T., Enochsson, O., Täljsten, B., and Elfgren, L. (2012). "Photographic strain monitoring during full-scale failure testing of Örnsköldsvik bridge." *Structural Health Monitoring*, 11(4), 489-498.

Smith, B., Kurama, Y., McGinnis, M. (2011). "Design and Measured Behavior of a Hybrid Precast Concrete Wall Specimen for Seismic Regions." *Journal of Structural Engineering*, 137(10), 1052-1062.

SS-EN 12390-3:2009 (2009). "Testing hardened concrete – Part 3: Compressive strength of test specimens." Swedish Standards Institute (SIS), Stockholm, Sweden.

SS-EN ISO 898-1 (2013). "Mechanical properties of fasteners made of carbon steel and alloy steel - Part 1: Bolts, screws and studs with specified property classes - Coarse thread and fine pitch thread (ISO 898-1:2013)." Swedish Standards Institute (SIS), Stockholm, Sweden.

SS-EN ISO 4014 (2011). "Hexagon head bolts - Product grades A and B (ISO 4014:2011)." Swedish Standards Institute (SIS), Stockholm, Sweden.

SS-EN ISO 6892-1:2009 (2009). "Metallic materials – Tensile testing – Part 1: Method of test at room temperature (ISO 6892-1:2009)." Swedish Standards Institute (SIS), Stockholm, Sweden.

Tan, K. H. (2002). "Strength Enhancement of Rectangular Reinforced Concrete Columns using Fiber-Reinforced Polymer." *Journal of Composites for Construction*, 6(3), 175-183.

Tanwongsval, S., Maalej, M., and Paramasivam, P. (2003). "Strengthening of RC wall-like columns with FRP under sustained loading." *Materials and Structures*, 36(5), 282-290.

Tetta, Z. C., Koutas, L. N., and Bournas, D. A. (2016). "Shear strengthening of full-scale RC T-beams using textile-reinforced mortar and textile-based anchors." *Composites Part B: Engineering*, 95, 225-239.

Todut, C., Dan, D., and Stoian, V. (2015). "Numerical and experimental investigation on seismically damaged reinforced concrete wall panels retrofitted with FRP composites." *Composite Structures*, 119, 648-665.

Todut, C., Dan, D., and Stoian, V. (2014). "Theoretical and experimental study on precast reinforced concrete wall panels subjected to shear force." *Engineering Structures*, 80, 323-338.

Triantafillou, T. C., Choutopoulou, E., Fotaki, E., Skorda, M., Stathopoulou, M., and Karlos, K. (2016). "FRP confinement of wall-like reinforced concrete columns." *Materials and Structures*, 49(1), 651-664.

Täljsten, B. (1999). "Strengthening of existing concrete structures with carbon fibre fabrics or laminates. Design, material and execution." *Technical Rep. No. 2000:16,* Luleå Univ. of Technology, Luleå, Sweden.

Wu, Y.-F., and Wei, Y.-Y. (2010). "Effect of cross-sectional aspect ratio on the strength of CFRP-confined rectangular concrete columns." *Engineering Structures*, 32(1), 32-45.

Wu, Y.-F., Yun, Y., Wei, Y., and Zhou, Y. (2014). "Effect of Predamage on the Stress-Strain Relationship of Confined Concrete under Monotonic Loading." *Journal of Structural Engineering*, 140(12), 04014093.

List of figures

Fig. 11. Strain utilization of the steel reinforcement for reference specimens (Stage I) and pre-cracked strengthened specimens (Stage II): (a) with a small opening (I/II-S) and (b) with a large opening (I/II-L)

** Strains not recorded for strengthened specimens due to malfunction of the strain gauge*

Fig. 12. Strain utilization of the steel reinforcement for reference specimens (Stage I) and uncracked strengthened specimens (Stage III): (a) with a small opening (I/III-S) and (b) with a large opening (I/II-L).

** Strains not recorded for strengthened specimens due to malfunction of the strain gauge*

Fig. 13. Major strains detected by 3D-DIC analysis at peak loads of specimens: (a) I-S; (b) II-S; (c) III-S1; (d) III-S2; (e) I-L; (f) II-L (90% of peak load); (g) III-L1 and (h) III-L2

List of tables

Table 1

Table 1 Mechanical properties of the concrete and steel reinforcement

Batch	Concrete				Steel reinforcement							
	Compressive strength		Fracture energy		Yield				Tensile			
					Strength		Strain		Strength		Strain	
	f_c (MPa)	CoV (%)	G_F (N/m)	CoV (%)	f_y (MPa)	CoV (%)	ε_y (‰)	CoV (%)	f_u (MPa)	CoV (%)	ε_u (‰)	CoV (%)
Batch 1	62.8	3.2	168	11.9	632	0.35	2.8	8.45	693	0.40	4.87	4.82
Batch 2	64.4	2.8	228	12.5								

Table 2

Table 2 Summary of test results

Specimen	N_{test} (kN)	$\varepsilon_{u,frp}$ (‰) F1 T	F1 C	F2 T	F2 C	F3 T	F3 C	F4 T	F4 C	F5 T	δ_e (mm)	δ_u (mm)	μ_Δ	E_d (kNm)
I-C	2363										4.6	18.4	4.05	39.37
I-S	1500					-					8.5	27.4	3.21	34.21
I-L	1180										4.1	11.3	2.78	10.88
II-S	2241	0.88	0.23	0.87	0.10	0.70	0.08	1.38	– 0.18	1.51	9.1	18.0	1.97	31.23
II-L	1497	0.46	0.21	0.21	0.13	0.27	0.21	0.39	0.08	1.24	4.1	5.0	1.23	4.66
III-S1	2178	0.80	0.20	0.96	0.20	0.73	– 0.25	0.95	0.20	1.89	8.2	15.9	1.94	26.61
III-S2	2009	0.94	– 0.02	0.81	0.22	0.99	0.37	1.64	– 0.11	1.57	4.6	15.5	3.38	29.89
III-L1	1334	0.24	0.05	0.22	0.18	0.47	0.25	0.88	– 0.14	1.63	8.0	8.4	1.05	6.60
III-L2	1482	N/A	0.11	N/A	0.10	N/A	0.53	0.54	0.44	1.48	3.4	7.4	2.18	9.66

Figure 1

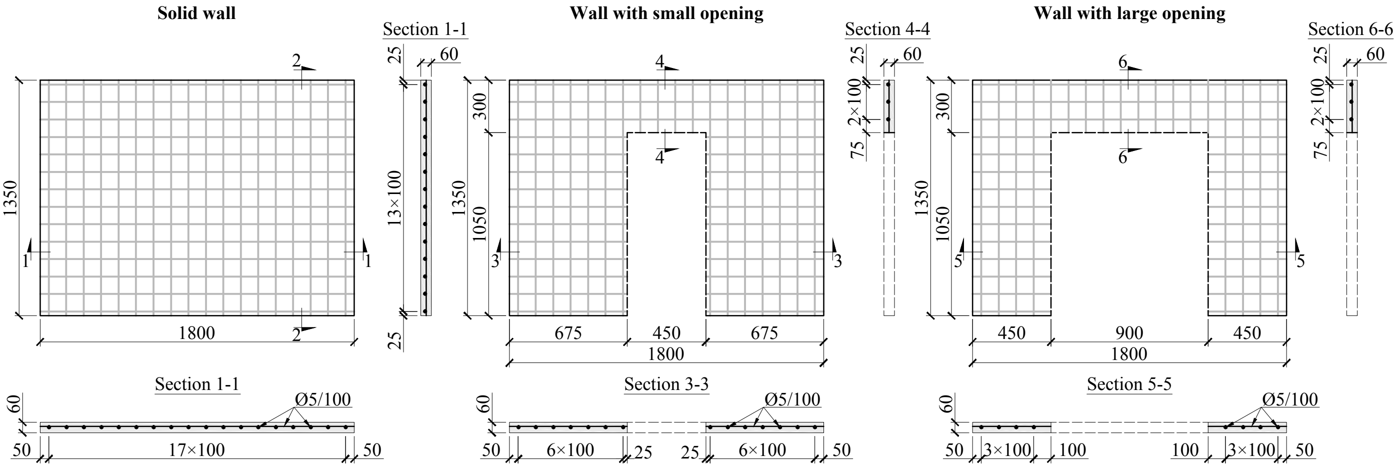

Solid wall
Section 1-1
Wall with small opening
Section 4-4
Wall with large opening
Section 6-6
1350
1800
13×100
25
60
300
1050
675
450
900
2×100
75
Section 1-1
Section 3-3
Section 5-5
Ø5/100
17×100
6×100
3×100
50
100

Figure 2a-c

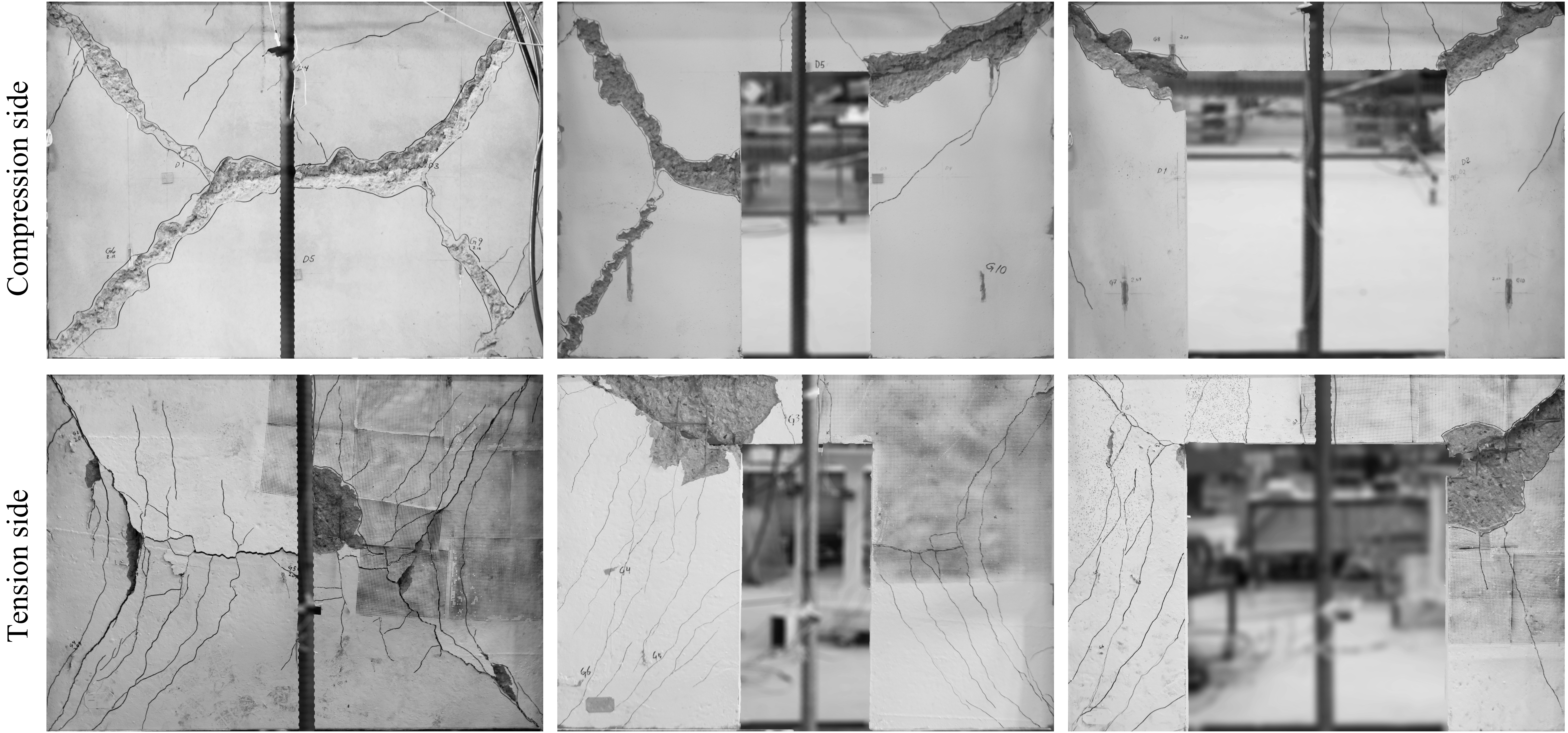

(a) (b) (c)

Figure 3

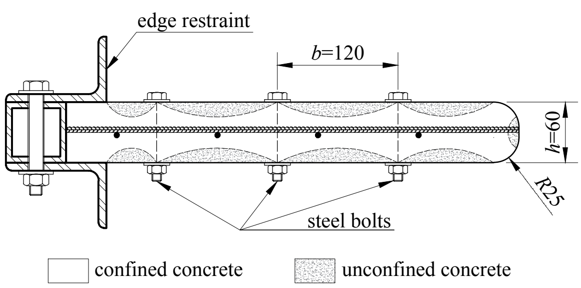
edge restraint
b=120
h=60
R25
steel bolts
confined concrete
unconfined concrete

Figure 4a-g

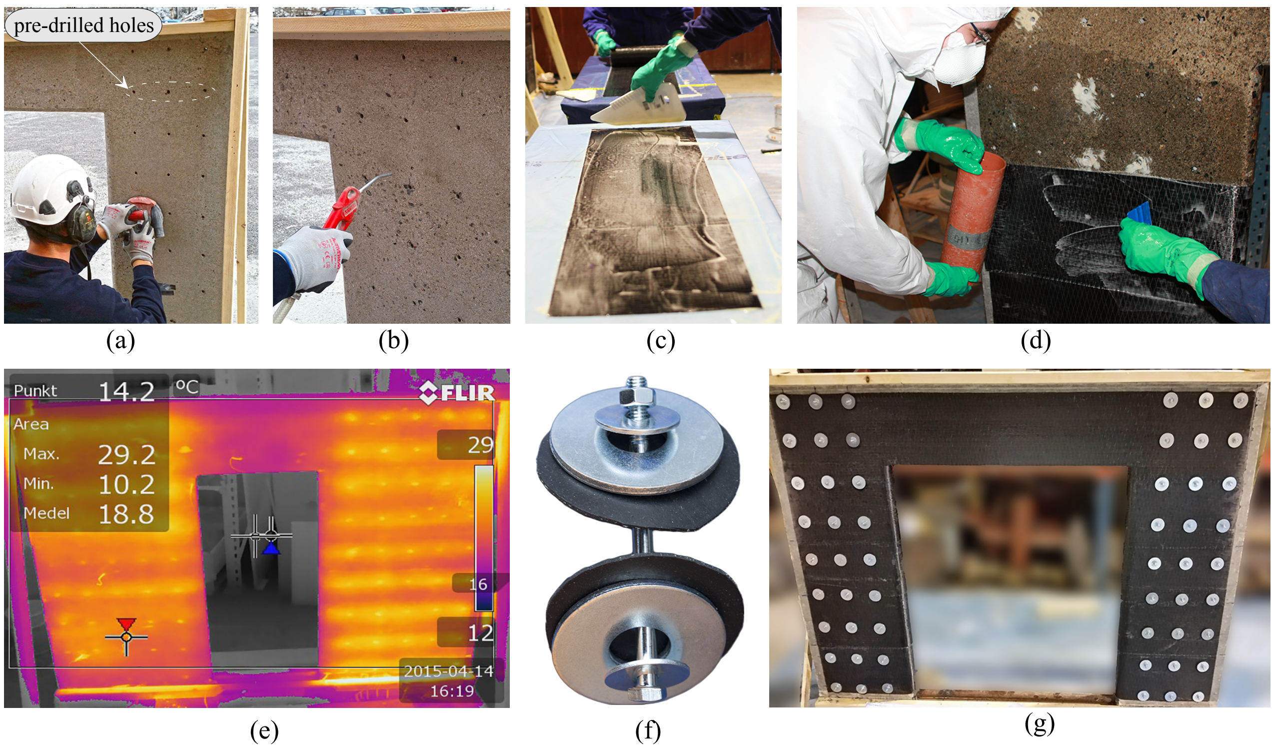

(a) (b) (c) (d) (e) (f) (g)

Figure 5

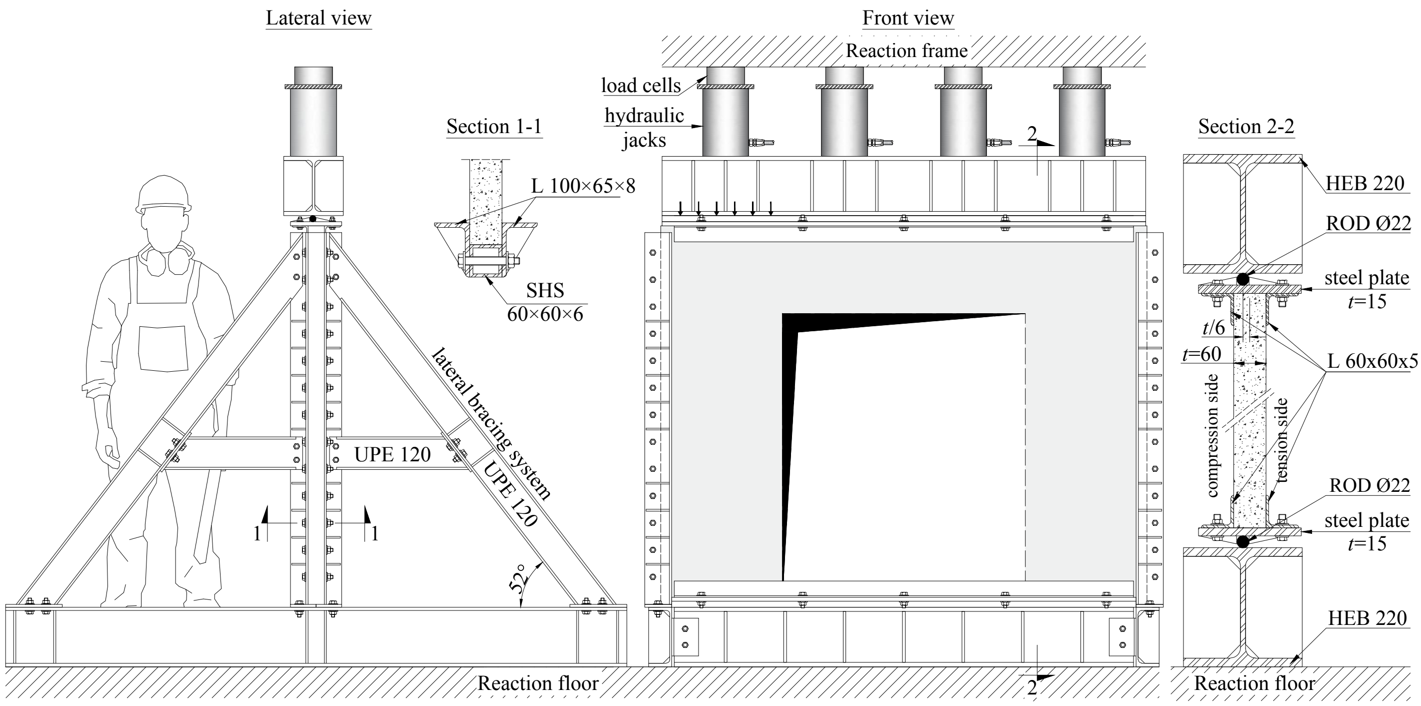

Lateral view
Section 1-1
L 100×65×8
SHS
60×60×6
UPE 120
lateral bracing system
UPE 120
1
1
52°
Reaction floor
Front view
Reaction frame
load cells
hydraulic
jacks
2
2
Section 2-2
HEB 220
ROD Ø22
steel plate
t=15
t/6
t=60
L 60x60x5
compression side
tension side
ROD Ø22
steel plate
t=15
HEB 220
Reaction floor

Figure 6

Figure 7

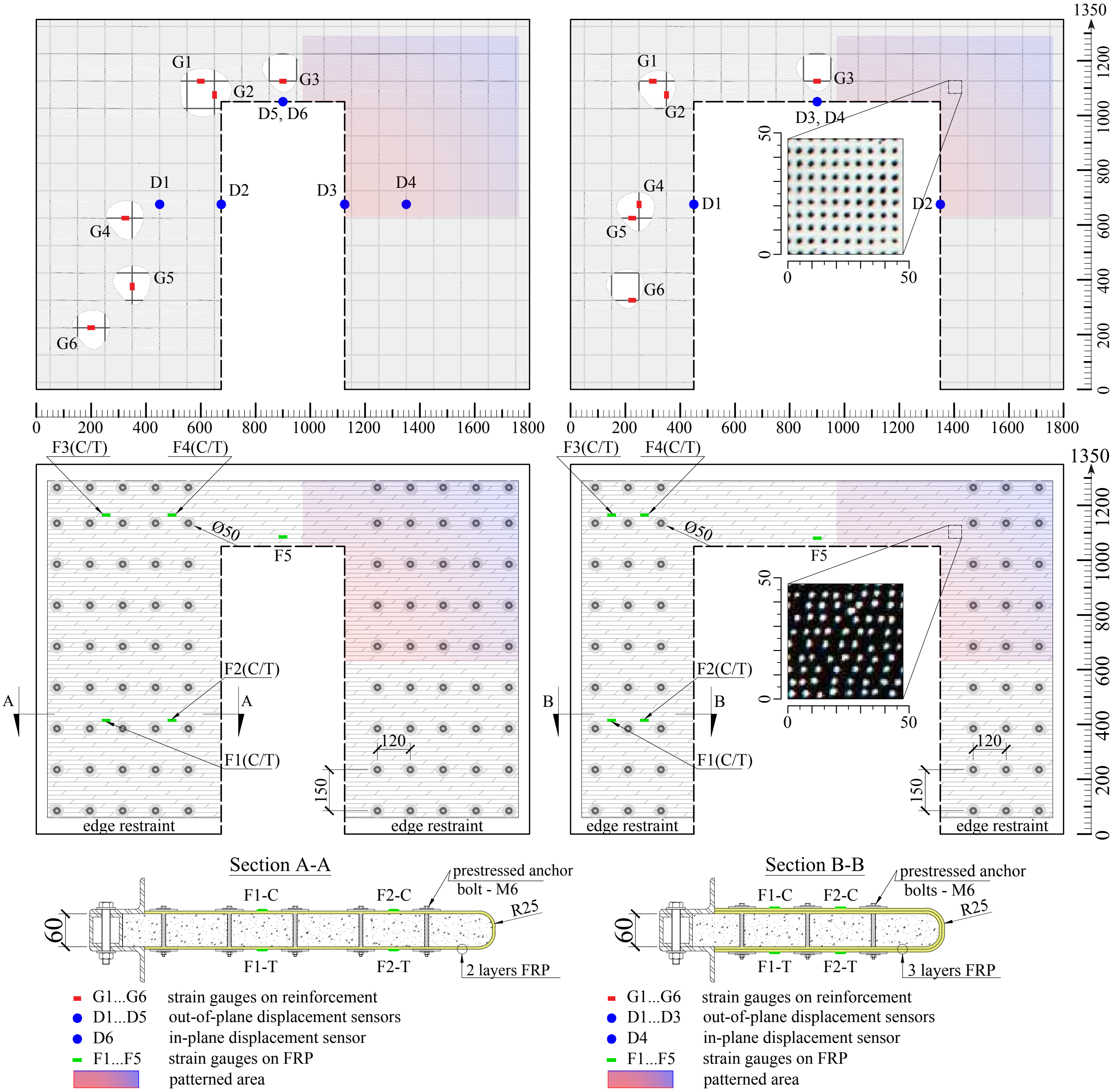

G1...G6 strain gauges on reinforcement
D1...D5 out-of-plane displacement sensors
D6 in-plane displacement sensor
F1...F5 strain gauges on FRP
patterned area
Section A-A
prestressed anchor bolt - M6
2 layers FRP
Section B-B
prestressed anchor bolts - M6
3 layers FRP
G1...G6 strain gauges on reinforcement
D1...D3 out-of-plane displacement sensors
D4 in-plane displacement sensor
F1...F5 strain gauges on FRP
patterned area
edge restraint

Figure 8

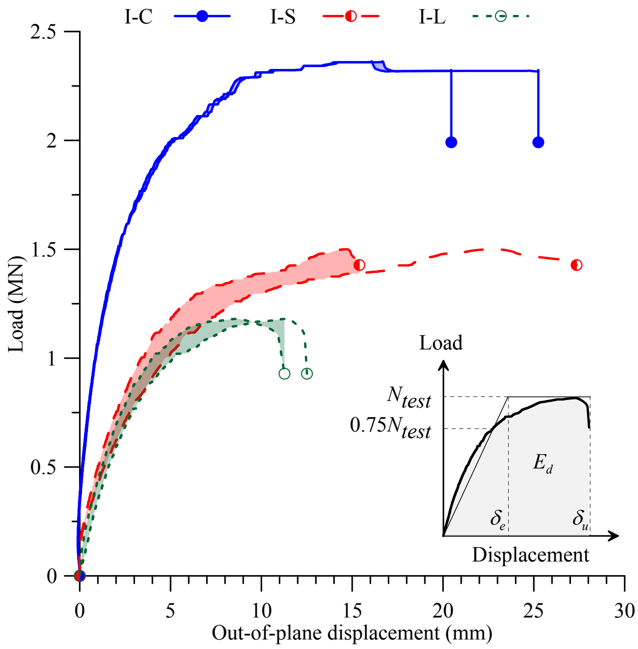

I-C
I-S
I-L
Load (MN)
2.5
2
1.5
1
0.5
0
0
5
10
15
20
25
30
Out-of-plane displacement (mm)
Load
N_{test}
$0.75N_{test}$
E_d
δ_e
δ_u
Displacement

Figure 9a-f

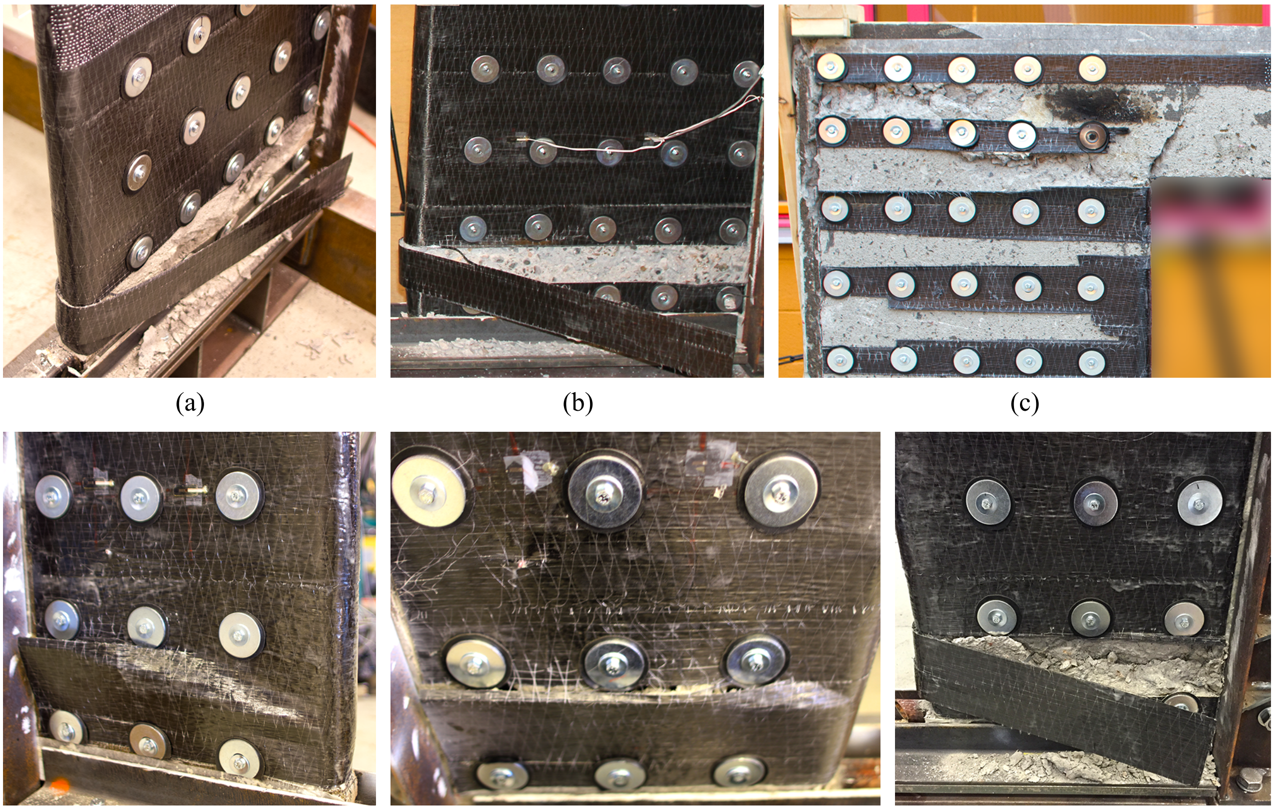

(a) (b) (c)

(d) (e) (f)

Figure 10a

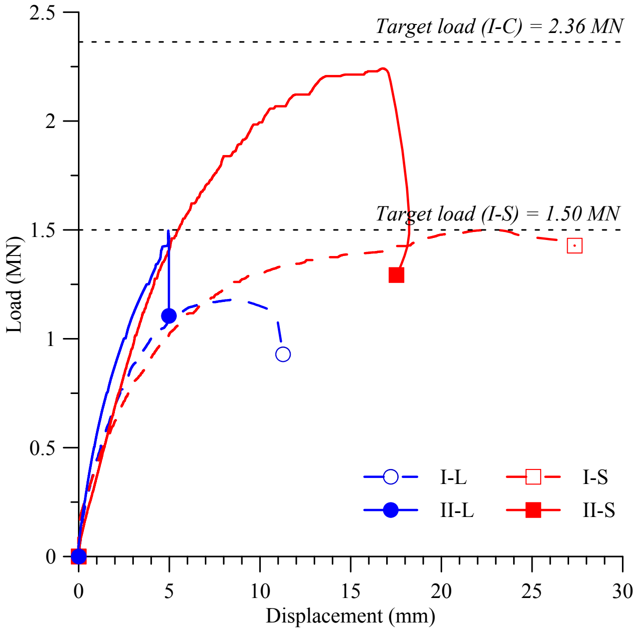

Target load (I-C) = 2.36 MN
Target load (I-S) = 1.50 MN
Load (MN)
Displacement (mm)
I-L
II-L
I-S
II-S
0
0.5
1
1.5
2
2.5
0
5
10
15
20
25
30

Figure 10b

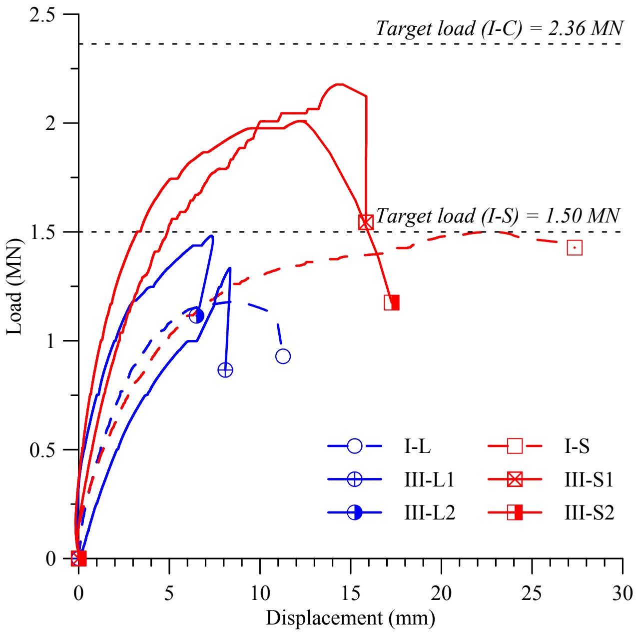

Target load (I-C) = 2.36 MN
Target load (I-S) = 1.50 MN
Load (MN)
Displacement (mm)
0
0.5
1
1.5
2
2.5
0
5
10
15
20
25
30
I-L
III-L1
III-L2
I-S
III-S1
III-S2

Figure 11a

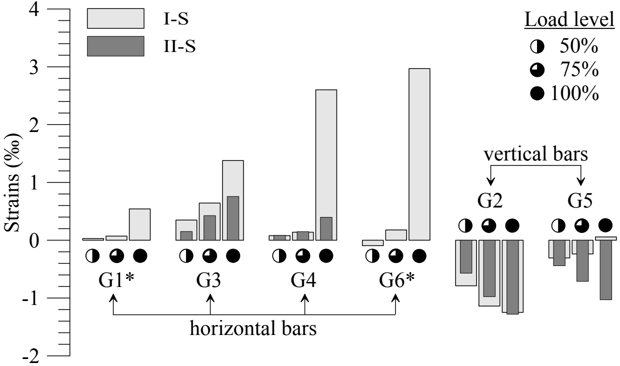
I-S
II-S
Load level
50%
75%
100%
Strains (‰)
4
3
2
1
0
-1
-2
vertical bars
G2
G5
G1*
G3
G4
G6*
horizontal bars

Figure 11b

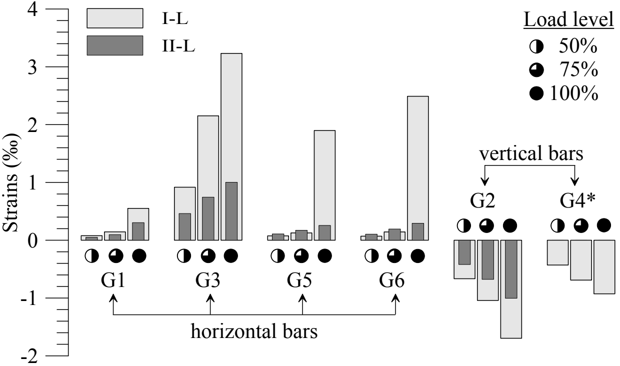

4
3
2
1
0
-1
-2
Strains (‰)
I-L
II-L
Load level
50%
75%
100%
G1
G3
G5
G6
horizontal bars
vertical bars
G2
G4*

Figure 12a

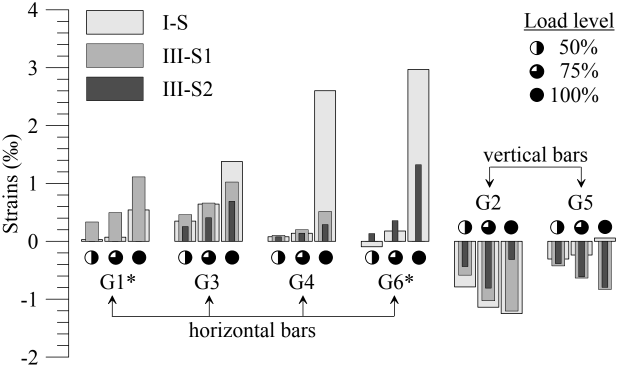

Strains (‰)
4
3
2
1
0
-1
-2
I-S
III-S1
III-S2
Load level
50%
75%
100%
G1*
G3
G4
G6*
horizontal bars
vertical bars
G2
G5

Figure 12b

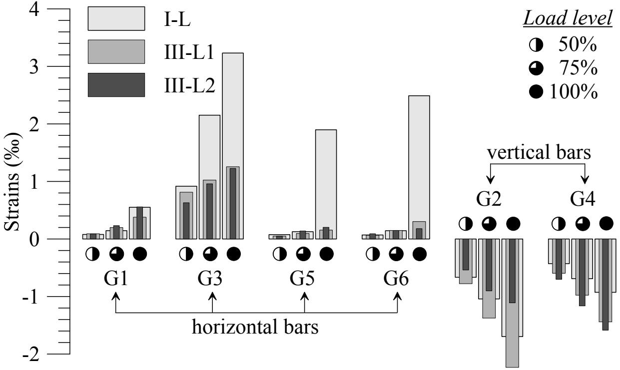

4
3
2
1
0
-1
-2
Strains (‰)
I-L
III-L1
III-L2
Load level
50%
75%
100%
G1
G3
G5
G6
horizontal bars
vertical bars
G2
G4

Figure 13a-h

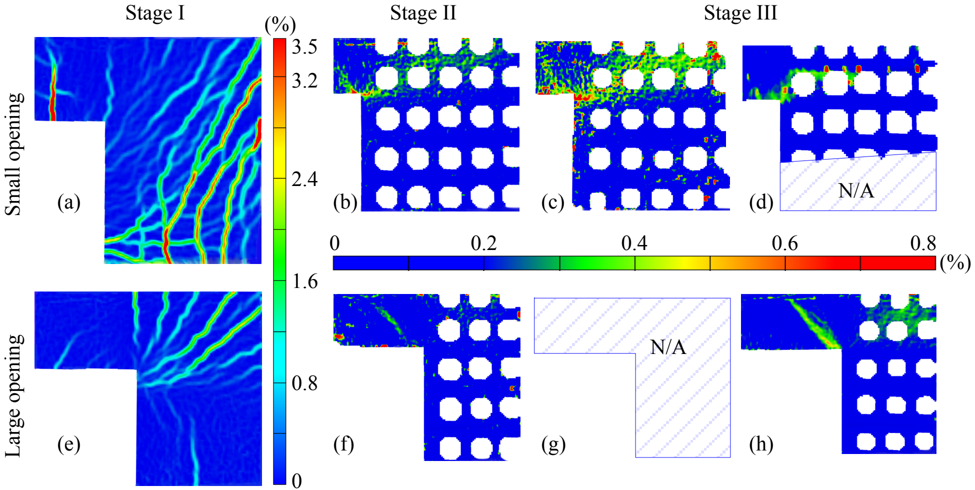

Stage I
Stage II
Stage III
(%)
3.5
3.2
2.4
1.6
0.8
0
Small opening
Large opening
(a)
(b)
(c)
(d)
N/A
0
0.2
0.4
0.6
0.8
(%)
(e)
(f)
(g)
N/A
(h)